ChemComm

ROYAL SOCIETY OF CHEMISTRY

COMMUNICATION

View Article Online
View Journal | View Issue

Cite this: *Chem. Commun.*, 2019, **55**, 5579

Received 8th February 2019,
Accepted 11th April 2019

DOI: 10.1039/c9cc01150a

rsc.li/chemcomm

Optimizing electron transfer from CdSe QDs to hydrogenase for photocatalytic H_2 production†

Monica L. K. Sanchez,[a] Chang-Hao Wu,[b] Michael W. W. Adams[b] and R. Brian Dyer *[a]

A series of viologen related redox mediators of varying reduction potential has been characterized and their utility as electron shuttles between CdSe quantum dots and hydrogenase enzyme has been demonstrated. Tuning the mediator LUMO energy optimizes the performance of this hybrid photocatalytic system by balancing electron transfer rates of the shuttle.

Artificial photosynthetic systems usually employ separate modules to accomplish the essential functions of efficient light harvesting, charge separation and catalytic proton coupled electron transfer (PCET) reactions to generate high energy chemical bonds.[1–3] This approach mimics the natural photosynthetic systems and allows independent optimization of each module for its specific task. Hybrid quantum-dot/enzyme photocatalysts are promising examples of this modular approach.[3–5] The nano-crystalline semiconductor (NCS) material acts as both the light harvesting and charge separation module. It can be designed to generate long-lived reductive or oxidative equivalents with high quantum efficiency. Enzymes that catalyze PCET reactions operate with little overpotential at rates that match or exceed the rate of generation of redox equivalents by the solar flux.[6] Thermophilic enzymes have high stability and durability, yielding high turnover numbers (TONs).[7] These modules have been highly optimized; however, the difficult challenge that remains is how to transfer reactive electrons between the modules. Both natural and artificial systems have employed redox mediators, small molecule electron carriers capable of moving between modules and efficient redox cycling. The challenges with this approach include generating a sufficient driving force for multiple electron transfer (ET) steps and efficient interfacial ET and avoiding back ET.[8] Methyl viologen (MV) and closely related molecules have been widely employed as electron relays largely because of their stable, long-lived radicals, commercial availability and solubility in water.[9–12] Most studies aimed at optimizing ET to and from a mediator have focused on manipulating the light harvesting/charge separation material.[9,10] Not much attention has been paid to tuning the mediator structure and redox potential for improving ET efficiency.[8,12,13] Here, we have investigated the effects of a mediator structure and reduction potential on the overall efficiency of a hybrid CdSe quantum-dot/mediator/[NiFe]-hydrogenase photocatalytic system. We varied the structure of viologen-like mediators by introducing methyl substituents and a carbon chain linking the two pyridyl nitrogens, as shown in Fig. 1. These modifications expand the range of reduction potentials of the mediators. We characterized this series of mediators structurally, spectroscopically and electrochemically and determined the effects of these mediator properties on the

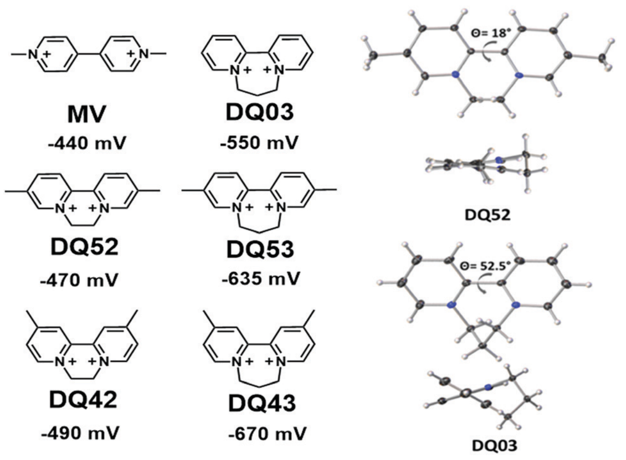

Fig. 1 Viologen-like molecules utilized as electron shuttles, along with electrochemically determined reduction potentials (*vs.* NHE). The numbering scheme refers to the position of the methyl substituents (4 or 5) and the length of the carbon chain (2 or 3). The X-ray structures (right) of DQ52 and DQ03 show how the twist angle depends on the carbon-linker chain length.

---

[a] *Department of Chemistry, Emory University, Atlanta, GA 30322, USA. E-mail: briandyer@emory.edu*

[b] *Department of Biochemistry and Molecular Biology, University of Georgia, Athens, GA 30602, USA*

† Electronic supplementary information (ESI) available: Experimental details, additional structural and spectral characterization of mediators and QDs, and quantum efficiency measurements. CCDC 1896282–1896286. For ESI and crystallographic data in CIF or other electronic format see DOI: 10.1039/c9cc01150a

photocatalytic production of hydrogen in the hybrid QD/hydrogenase system.

The mediator structure influences its performance as an electron shuttle in several ways. The position of the pyridyl methyl substituent affects both the electronic structure of the mediator and the sterics of its interaction with a nanocrystalline semiconductor surface. The carbon chain linking the two pyridyl nitrogens introduces a twist in the torsion angle of the two rings that depends on the chain length. Evidence of the twist along the bipyridine core is clear from the X-ray structures (Fig. 1) and the NMR spectra (Fig. S1, ESI†) of the mediators and is consistent with previous reports.[14] Representative X-ray structures for DQ52 and DQ03 are presented in Fig. 1 (detailed structural information for all mediators are given in Tables S1 and S2, ESI†). The average torsional twist between the pyridyl rings was ~19° for those mediators with a two-carbon chain linker and ~53° for those with a three-carbon chain linker. The torsional twist also causes important changes in the electronic structure of the mediators. These changes are reflected in the reduction potential, which becomes more negative as the torsional twist increases. Previous molecular orbital (MO) calculations for mediators with 2C and 3C linkers showed that increasing the torsional twist disrupts the conjugated system and shifts the LUMO to a higher energy.[14] The effect on the mediator electronic structure is also reflected in the UV-vis absorbance spectra of the di-cation and mono-cation forms (Fig. 2 and Fig. S2, ESI†). The $\pi \rightarrow \pi^*$ transition of the di-cation is observed to shift to higher energy with an increasing torsional twist.[15] This blue shift is related to the change in ΔE between the HOMO and LUMO with the twist angle. The MO calculations indicate that ΔE increases due to the increase in the LUMO energy, consistent with our observation of more negative reduction potentials in the cyclic voltammetry data (Fig. S3, ESI†).[14] In contrast, the $\pi \rightarrow \pi^*$ transition of the reduced mediators is observed to shift to lower energy with an increasing linker length (Fig. 2A). This red-shift has been attributed previously to a more planar structure for the radical species.[14,15] The decrease in the torsional twist associated with the radical cation formation allows a greater degree of orbital overlap between the bipyridinium rings, leading to the lower energy transition. Slower ET rates are observed as the twist angle is increased, due to an increase in the reorganization energy required to reach the planar structure of the reduced state.[16] Electronic structure calculations of DQ03 also support a change in the geometry of the mediator from the twisted form to a more planar configuration upon reduction.[14]

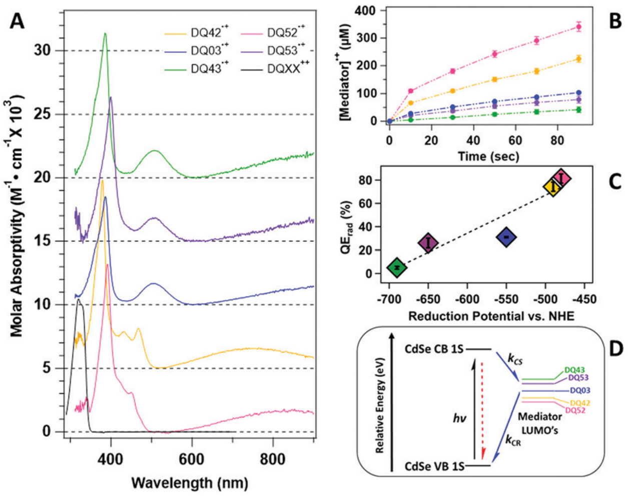

Fig. 2 Steady-state photoreduction experiments with CdSe QDs and mediators. (A) UV-vis extinction spectra for reduced mediators compared to oxidized DQ03^{2+}; spectra are offset for clarity. (B) Kinetics of photoreduction of the mediator, quantified by monitoring the absorbance at 450 or 510 nm for 2C or 3C linked radical species, respectively. (C) Dependence of quantum efficiency for reduction of mediators on reduction potential. (D) Schematic illustration of the ET processes and energies of the CdSe QD conduction band (CB) and the valence band (VB) relative to the mediator LUMO energies.

The first step in the electron shuttle process is ET from the conduction band (CB) of the excited CdSe QD to the mediator. We performed steady-state photo-illumination experiments to determine the quantum efficiency for reduction of the mediator (QE_{rad}) as shown in Fig. 2. Illumination of the CdSe QD with blue light (405 nm) produces an exciton state, which the mediator quenches by extracting an electron from the CB, generating a population of the reduced mediator radical cation (mediator$^{\bullet+}$). The hole left in the VB of the CdSe QD is scavenged by the sacrificial electron donor (SED), mercaptopropionic acid (MPA). This ET event (k_{CS}) is depicted schematically in Fig. 2D along with the relative LUMO energies of the mediators. The absorbance spectra of the radical cations are shown in Fig. 2A. The absorbance at either 450 nm or 510 nm was monitored for each mediator depending on whether the spectrum belonged to a 2C or 3C linked molecule, respectively. The concentration of the reduced mediator *versus* the illumination time (Fig. 2B) is determined from the measured extinction coefficient of each radical species. QE_{rad} was determined by dividing the moles of radicals generated by the moles of photons absorbed by the solution and correcting for reflection from the front face of the cuvette. We calculate the quantum yield from the first 10 seconds of illumination, before the concentration of mediator$^{\bullet+}$ builds up, thus minimizing contributions from back ET (k_{CR}) and other parasitic processes that lead to mediator degradation (full details of the calculation are presented in the ESI†).[7]

The rate of formation of mediator$^{\bullet+}$ is constant for the first 10 seconds but begins to decline after this initial phase (Fig. 2B). The decrease in the rate of formation of mediator$^{\bullet+}$ is attributed to the consumption of the mediator di-cation and to an increased rate of charge recombination at high concentrations of mediator$^{\bullet+}$. At longer time periods, the rate of mediator reduction and charge recombination are balanced and the system reaches a steady state. The initial rates of mediator$^{\bullet+}$ formation and steady state concentrations vary with the reduction potential of the mediator (Fig. 2B), with the 2C linker mediators having significantly faster initial rates and reaching larger steady state populations than the 3C linker ones. It is clear that the 2C linker molecules, DQ42 and DQ52, have the highest net QE_{rad} (Fig. 2C). The differences in QE_{rad} are best explained by considering the faster k_{CS} and the slower k_{CR} observed for the 2C linked mediators relative to the 3C linked ones. The result of the faster k_{CS} and the slower k_{CR} is a net higher QE_{rad} and therefore larger steady state populations of the reduced mediator, as strongly suggested by the steady-state data.

The differences in the ET rates and net QE_{rad} for this series of mediators can be understood in terms of the reduction potentials, which influence both the forward and reverse ET reactions.[17] Fig. 2C shows the dependence of the net QE_{rad} on the reduction potential of the mediator. The energetics of this process is illustrated in Fig. 2D, where the relative energy levels were determined from the reduction potentials of the mediators and the band edge of the CdSe QDs. The 2C linker mediators with more positive redox potentials (lower energy LUMOs) have a larger downhill driving force for forward ET and a smaller driving force for back ET, resulting in the larger k_{CS} and the smaller k_{CR} (normal Marcus regime). The net result is a long-lived charge separated state and a high QE_{rad}. The situation is more complex for the 3C linker mediators, since their more negative reduction potential yields a driving force for back ET in the Marcus inverted regime, resulting in a decrease in k_{CR}.

It is also likely that the rate of ET from the QD to the mediator and the net QE_{rad} are affected by the differences in the reorganization energy for forward and reverse ET across this series. The reorganization energy is influenced by the torsional twist between the pyridyl rings of the mediators, since the reduced mediator adopts a more planar structure.[16] Thus, the reorganization energy for the more highly twisted 3C linker molecules is expected to be larger than that for the 2C linker molecules. This increased reorganization energy is expected to slow down the ET to the 3C linker molecules relative to the 2C linker ones, leading to less efficient charge separation. For example, the net QE_{rad} drops dramatically from 74% to 31% between DQ42 and DQ03 as the twist in the bipyridyl core is increased from ∼22° to ∼55°. A further study would be required to assess the relative contributions of the reorganization energy and the driving force to the difference in the net QE_{rad}, but both are likely important.

The next step in the electron shuttle process is ET from the mediator$^{\bullet+}$ to the hydrogenase and the turnover of the enzyme to produce hydrogen. We measured the hydrogen production efficiency for a hybrid system consisting of CdSe QDs, mediator and the [NiFe] SHI from *Pyrococcus furiosus* (*Pf*) as the hydrogen production catalyst. *Pf* SHI is a robust catalyst, having high thermal stability and oxygen tolerance.[18] It also has a high turnover rate at neutral pH (100 s^{-1} at room temperature) and operates close to the thermodynamic potential of the hydrogen couple. Hydrogen production assays were carried out at pH 7.1 under conditions analogous to those used in the mediator photoreduction experiments. Fig. 3A shows the time-dependent yields of light driven hydrogen production for each of the mediators. Furthermore, addition of a mediator to this hybrid system significantly improves the overall quantum yield for hydrogen production compared to related systems that rely on direct ET from the NCS material to the hydrogenase. The net production of H_2 and the corrected QE_{hyd} for each mediator are summarized in Table 1.

Trends in the QE_{hyd} indicate a strong correlation between the reduction potential of the mediator and the amount of H_2 produced as shown in Fig. 3B. Previously, we investigated the effect of the mediator reduction potential on the efficiency of a related hybrid CdSe/CdS nanorod-hydrogenase photocatalytic system.[7] We compared two mediators, methyl viologen (MV^{2+}, $E_0 = -446$ mV *vs.* NHE) and DQ03 (or PDQ^{2+}, $E_0 = -550$ mV *vs.* NHE) and found a significantly better performance with DQ03, due to its greater driving force for ET to the surface exposed FeS cluster of SHI. With DQ03 and nanorods, we achieved the highest reported quantum yield for hydrogen production with such hybrid photocatalytic systems.[7] The current results are consistent with the previous ones, showing a greater overall efficiency of hydrogen production with an increased driving force for electron transfer from the reduced mediator to the enzyme. The highest observed quantum efficiency for H_2 production is modest ($QE_{hyd} = 16.8\%$) compared to previous results with nanorods ($QE_{hyd} = 52\%$ for similar conditions). This difference in efficiency is primarily due to the NCS photosensitizer, since the nanorod structure has a significantly longer exciton lifetime than the QD, leading to a greater efficiency of the charge separation process. Nevertheless, the yields for the three highest performing mediators in the present work are significantly higher than what has been observed previously with CdSe QDs.[19]

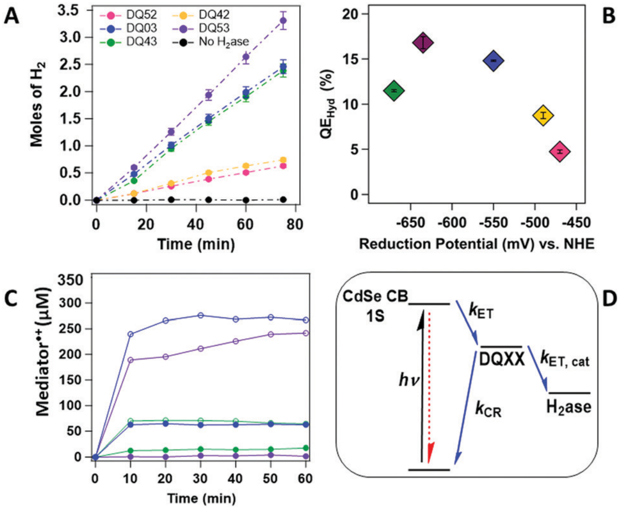

Fig. 3 Steady-state H_2 production. (A) H_2 production as a function of the laser illumination time: DQ53 (purple), DQ43 (green), DQ03 (blue), DQ42 (yellow), DQ52 (pink), and with no mediator (black). (B) Correlation of H_2 generation efficiency (QE_{hyd}) with reduction potential. (C) Production of the reduced mediator *versus* the illumination time with H_2ase (closed circles) and without H_2ase (open circles). (D) An energy diagram of ET steps.

Table 1 Steady state hydrogen production (at 5000 s)

Mediator	Solution potential (mV)[a]	Moles H_2	QE_{corr} (%)
DQ52	−375	4.1×10^{-7}	4.7
DQ42	−385	8.1×10^{-7}	7.8
DQ03	−410	2.7×10^{-6}	14.8
DQ53	−425	3.7×10^{-6}	16.8
DQ43	−495	2.6×10^{-6}	11.5

[a] *Versus* SHE; determined from the Nernst equation: $\Delta E = \Delta E^{\circ} - \frac{RT}{F}\ln\frac{[\mathrm{Med}^{+\bullet}]}{[\mathrm{Med}^{2+}]}$.

The correlation of photocatalytic hydrogen production efficiency with reduction potential of the mediator is inverse to the trend observed for the steady-state mediator photoreduction experiments. This observation highlights the complex interplay between the net yield of hydrogen production and the rates of charge separation, charge recombination and ET to the enzyme, as shown in the scheme in Fig. 3D. Optimum hydrogen production requires a balance between the driving force for the two forward ET processes; decreasing the mediator LUMO energy decreases the driving force for the ET to the catalyst (k_{ET}), but at the same time increases the driving force for reduction of the mediator (k_{CS}). Thus, while the mediators that are easier to reduce (lower LUMO energies) exhibit a higher quantum efficiency for photoreduction by the QDs, they are less effective in reducing the enzyme and producing hydrogen. In contrast, charge recombination becomes more rapid as the LUMO energy is increased, which lowers the net yield of photoreduction in the absence of enzyme. In the presence of enzyme, however, ET to the enzyme is competitive with charge recombination and thus efficient hydrogen production can be achieved.

Further insight into the optimum parameters for hydrogen production is provided by considering the solution potential achieved under illumination at a steady state. Fig. 3C shows the production of the reduced mediator as a function of the illumination time for DQ03, DQ43, and DQ53 mediators with and without hydrogenase. The reduced mediator concentration increases initially, and then reaches a constant value; a lower steady state population is reached in the presence of hydrogenase, due to the ET to the enzyme. It is clear that in all cases the system reaches the steady state (constant mediator$^{\bullet+}$ concentration) within an hour. Therefore, we determined the steady state solution potential by measuring the concentration of the reduced mediator from the radical absorbance after 5000 s of illumination. The Nernst equation was then used to calculate the solution potential from the relative concentration of the mediator$^{\bullet+}$/mediator^{++}, yielding values shown in Table 1. For comparison, at pH 7.1 the hydrogen couple is at −419 mV. The most efficient mediators DQ03, DQ53 and DQ43 reach steady state solution potentials close to or more negative than the hydrogen couple. In contrast, with DQ42 and DQ52 the steady state solution potentials are significantly more positive than the hydrogen couple and therefore proton reduction is not favorable for the 2C linker mediators.

The hydrogen production efficiency peaks with DQ53 even though it does not have the most negative reduction potential. DQ53$^{\bullet+}$ concentration levels close to those observed for DQ03$^{\bullet+}$ are achieved when the solution contains solely dots and mediator (Fig. 3C). When the enzyme is present, however, steady state illumination produces a barely observable population of DQ53$^{\bullet+}$, indicating that its consumption by the enzyme is rapid. Based on this evidence, it is likely that the conditions are not fully optimized for hydrogen production in the case of DQ53. Utilization of a photosensitizer with a longer-lived exciton, such as a nanorod, would increase the QE_{hyd} produced with DQ53, since it would increase QE_{rad}. The lower QE_{hyd} observed with DQ43 is in part due to the inefficient ET to the enzyme despite its more negative reduction potential, resulting in a higher steady state population of the mediator$^{\bullet+}$ compared to DQ53 (Fig. 3C). A slower ET to the enzyme for DQ43 might be an indication of entrance into the Marcus inverted regime, wherein having an increased driving force slows the ET to the enzyme, resulting in a lower than expected QE_{hyd}.

In this report, we have optimized the hydrogen production efficiency of a hybrid photocatalytic system consisting of a nanocrystalline semiconductor (CdSe QD) photosensitizer and a hydrogenase enzyme (*Pf* SHI). The performance was optimized by tuning the structure and reduction potential of the redox mediator that serves as an electron shuttle between the QD and enzyme. Optimum performance requires a careful balance among the rates of charge separation, ET to the enzyme and charge recombination, which can be achieved by tuning the energy of the mediator LUMO. The versatility of this modular system makes it attractive for additional studies with other photosensitizer materials and with other biological or man-made catalysts for PCET processes such as CO_2 reduction.

The authors thank Dr John Bacsa for help with X-ray crystal structure determination. Funding for this work was provided by the National Science Foundation (grants CHE1807865 and DMR1808288 to RBD) and by the Division of Chemical Sciences, Geosciences and Biosciences, Office of Basic Energy Sciences of the U. S. Department of Energy (grant DE-FG05-95ER20175 to MWA).

Conflicts of interest

There are no conflicts to declare.

Notes and references

1 K. A. Brown, D. F. Harris, M. B. Wilker, A. Rasmussen, N. Khadka, H. Hamby, S. Keable, G. Dukovic, J. W. Peters, L. C. Seefeldt and P. W. King, *Science*, 2016, **352**, 448–450.
2 M. Đokić and H. S. Soo, *Chem. Commun.*, 2018, **54**, 6554–6572.
3 B. L. Greene, C. A. Joseph, M. J. Maroney and R. B. Dyer, *J. Am. Chem. Soc.*, 2012, **134**, 11108–11111.
4 K. A. Brown, M. B. Wilker, M. Boehm, H. Hamby, G. Dukovic and P. W. King, *ACS Catal.*, 2016, **6**, 2201–2204.
5 K. A. Brown, S. Dayal, X. Ai, G. Rumbles and P. W. King, *J. Am. Chem. Soc.*, 2010, **132**, 9672–9680.
6 T. W. Woolerton, S. Sheard, Y. S. Chaudhary and F. A. Armstrong, *Energy Environ. Sci.*, 2012, **5**, 7470–7490.
7 B. Chica, C.-H. Wu, Y. Liu, M. W. W. Adams, T. Lian and R. B. Dyer, *Energy Environ. Sci.*, 2017, **10**, 2245–2255.
8 M. S. Kodaimati, K. P. McClelland, C. He, S. Lian, Y. Jiang, Z. Zhang and E. A. Weiss, *Inorg. Chem.*, 2018, **57**, 3659–3670.
9 H. Zhu, N. Song, H. Lv, C. L. Hill and T. Lian, *J. Am. Chem. Soc.*, 2012, **134**, 11701–11708.
10 E. A. Weiss, *ACS Energy Lett.*, 2017, **2**, 1005–1013.
11 M. D. Peterson, S. C. Jensen, D. J. Weinberg and E. A. Weiss, *ACS Nano*, 2014, **8**, 2826–2837.
12 A. J. Morris-Cohen, M. D. Peterson, M. T. Frederick, J. M. Kamm and E. A. Weiss, *J. Phys. Chem. Lett.*, 2012, **3**, 2840–2844.
13 J. Chen, K. Wu, B. Rudshteyn, Y. Jia, W. Ding, Z.-X. Xie, V. S. Batista and T. Lian, *J. Am. Chem. Soc.*, 2016, **138**, 884–892.
14 S. H. R. Brienne, P. D. W. Boyd, P. Schwerdtfeger, G. A. Bowmaker and R. P. Cooney, *J. Mol. Struct.*, 1995, **356**, 81–94.
15 S. Yasui, K. Itoh, A. Ohno and N. Tokitoh, *Org. Biomol. Chem.*, 2006, **4**, 2928–2931.
16 R. F. Anderson and K. B. Patel, *J. Chem. Soc., Faraday Trans.*, 1984, **80**, 2693–2702.
17 H. Zhu, Y. Yang, K. Wu and T. Lian, *Annu. Rev. Phys. Chem.*, 2016, **67**, 259–281.
18 B. L. Greene, C.-H. Wu, P. M. McTernan, M. W. W. Adams and R. B. Dyer, *J. Am. Chem. Soc.*, 2015, **137**, 4558–4566.
19 S. Kundu and A. Patra, *Chem. Rev.*, 2017, **117**, 712–757.